ACS APPLIED MATERIALS & INTERFACES

www.acsami.org

Research Article

Energy Harvesting Using ZnO Nanosheet-Decorated 3D-Printed Fabrics

Partha Kumbhakar,[#] Rushikesh S. Ambekar,[#] Arko Parui,[#] Ajit K. Roy, Debmalya Roy,[*] Abhishek K. Singh,[*] and Chandra S. Tiwary[*]

Cite This: *ACS Appl. Mater. Interfaces* 2023, 15, 44513−44520

Read Online

ACCESS | Metrics & More | Article Recommendations | Supporting Information

ABSTRACT: In this work, we decorated piezoresponsive atomically thin ZnO nanosheets on a polymer surface using additive manufacturing (three-dimensional (3D) printing) technology to demonstrate electrical−mechanical coupling phenomena. The output voltage response of the 3D-printed architecture was regulated by varying the external mechanical pressures. Additionally, we have shown energy generation by placing the 3D-printed fabric on the padded shoulder strap of a bag with a load ranging from ∼5 to ∼75 N, taking advantage of the excellent mechanical strength and flexibility of the coated 3D-printed architecture. The ZnO coating layer forms a stable interface between ZnO nanosheets and the fabric, as confirmed by combining density functional theory (DFT) and electrical measurements. This effectively improves the output performance of the 3D-printed fabric by enhancing the charge transfer at the interface. Therefore, the present work can be used to build a new infrastructure for next-generation energy harvesters capable of carrying out several structural and functional responsibilities.

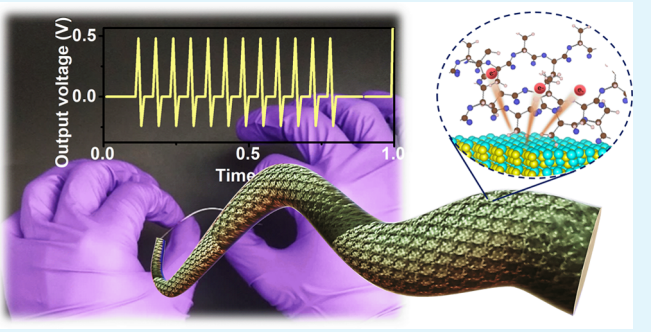

KEYWORDS: *two-dimensional ZnO, 3D printing, interface, energy harvesting, nanogenerator*

1. INTRODUCTION

One of the most critical factors for the survival of humankind is sustainable green energy. Fast industrialization and population growth have increased the need for energy globally.[1−3] The demand for renewable energy is growing daily, including biomass, geothermal, wind, solar, hydropower, and other sources.[4] The process that transforms mechanical energy into electric energy is termed the piezoelectric-based green energy harvesting system.[5−7] Researchers have attempted to develop complex structures of the substrate as there are numerous ways to modify the piezoelectricity of materials, including the tuning of ultrathin geometry, coating with two-dimensional (2D) materials, good electromechanical responsiveness, and other unique physical qualities, including enlarged surface area.[6] These complex structures can be fabricated via the three-dimensional (3D) printing technique, which can be used as a template for energy harvesting. 3D printing provides flexibility in designing complex structures with several advantages such as zero wastage, environment-friendly, economical, and high-end automation.[7]

Because of the numerous potential applications in the near future, such as medical monitoring devices or implants, portable military equipment, and smart textiles with integrated electronic functionalities, flexible and wearable electronics are gaining more and more interest in academia and industry.[8−10] Numerous fiber- and planar-shaped electrochemical energy storage devices reported in the literature have promising electrochemical and mechanical properties and are constructed on flexible substrates like metal sheets, wires, plastic thin films and fibers, papers, and textile materials.[8,9,11] When considering energy storage technologies, particularly those that are targeted at wearable applications, material properties such as flexibility and durability, safety, scalability, and integration are crucial parameters to be considered. The output efficiency of the device depends on the effective contact area, disparity in electrical polarities, etc. Studying the high aerial device performance on fabric platforms has been difficult while maintaining the optimized device dimensions and mechanical flexibility for wearable applications.

Nanoscale electronic device systems and energy harvesting applications are promising for two-dimensional (2D) layered materials. In recent years, interest in 2D materials made of piezoelectric, flexoelectric, triboelectric, and hybrid system has increased.[12,13] For emerging wearable electronics technologies, 2D materials are widely used due to their weak interlayer

Received: June 13, 2023
Accepted: August 15, 2023
Published: September 12, 2023

contacts, van der Waals (vdW) interactions, easily connected with the external surface, and high flexibility.[14−18] In fact, 2D material/soft matter interfaces have been used in the transfer, printing, and processing of various electronic technologies. These interfaces are crucial for controlling the structural and morphological aspects, adjusting the physical properties, and enhancing the functionality of flexible devices made of soft substrates. Covalent bonding might enhance the adherence of 2D layers to external surfaces at the interfaces. However, the packing and coating of 2D materials on different surfaces provide trade-off challenges, and the management of interfacial instability is essential to the success of protective layers. Various coating techniques (spray coating, spin coating, and dip coating) are available to coat the 2D materials on 3D-printed structures. Among all, dip coating is the easy and suitable technique by considering the complexity of the structure. The thickness of coating layers depends on the concentration of the nanomaterial and the number of times complex structures dipped in the solution.[19] 2D material-decorated 3D-printed polymeric structures can be an excellent solution in which nanomaterials exert piezoelectricity, and the complex structure provides the extended area with optimum flexibility or rigidity to the entire architecture.[20] These 3D-printed coated architecture can be used in muscle movement during walking/running and efficiently utilized to power low-consumable electronic gadgets, specifically in remote areas such as high terrains, mines, caves, etc.[21] Additionally, as a flexible architecture, bags are an essential component of daily living. Backpacks are frequently used for transportation, fashion, sports, business, education, shopping, healthcare, etc. It has a wide range of applications across different industries and contexts. Therefore, integrating the energy harvesting device with bags will pave the way for a green, self-powered energy source.

Here, an in situ ZnO-decorated 3D-printed flexible architecture was developed for energy harvesting applications. The ZnO nanosheets were grown on a 3DP fabric and characterized by optical and microscopic measurements. The 3D-printed architecture provides flexibility, strong adhesion, tunable specific surface area, and load-bearing capability without failure. The piezoelectric−triboelectric combined response of the 3DP system against different variables like the magnitude of force, various types of forces, and UV light intensity has been studied. The real-time application of the as-developed structure was demonstrated at the padded shoulder strap of the bag. This study paves the way for a class of rationally designed electromechanical coupling materials, thus moving structural materials toward smart infrastructures. In order to utilize the piezoelectric−triboelectric interface, a DFT calculation was carried out of the composite system.

2. EXPERIMENTAL DETAILS

2.1. Experimental Methods. The poly(lactic acid) (PLA) filament was provided by Flashforge 3D Technology Co. Ltd. (Zhejiang, China). It has a 1.75 mm diameter with a ±0.05 mm tolerance. It melts between 190 and 220 °C and has a density of 1.25 ± 0.05 g/cm^3. First, the PLA filament is fed into the Flashforge Adventure 3 3D printer through guide pipes. The extruder temperature was kept at 210 °C, and the bed temperature was at 50 °C. The structure was printed at hyper-resolution in which the first layer height was 200 μm and the remaining layer height was 80 μm. To increase the surface area of the overall structure, 60% infill was used with a hexagonal pattern, which was also optimized without damaging the structural geometry. The standard travel speed (70 mm/s) and print speed (40 mm/s) have been maintained. The printed structure solidifies at room temperature with external fan cooling. The 3D-printed hex structure before and after printing is shown in Figure 1. We have carried out the optical imaging

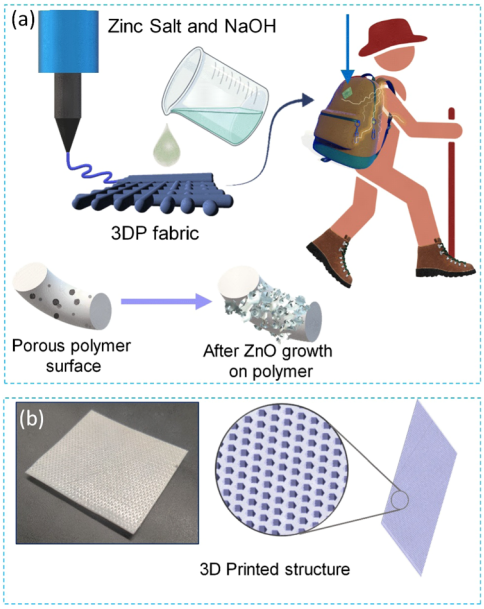

Figure 1. (a) Schematic representation of the synthesis procedure of in situ ZnO growth on 3D-printed structures. Before and after coating of a porous polymer substrate (lower panel). (b) Digital photograph and 3D-printed image of the fabric.

by capturing micrographs before and after treatment of the 3D-printed PLA hex structures with NaOH/ethanol solution. We found that the structural features are mostly unaltered by the treatment of dilute base solution; however, the higher pH enhanced the surface roughness of the fabric, which in turn, promotes surface adhesion and growth of ZnO on PLA fabrics (Figure S1).

The wet chemical synthesis route (Figure 1a) was used to grow ZnO nanosheets on the 3D-printed hex structure. Then, the structure was immersed in the zinc(II) nitrate (0.5 M)/water−ethanol mixture (20 mL). NaOH/ethanol solution of 30 mg/mL concentration was added dropwise to achieve ZnO nanosheets. The solution was kept at 60 °C temperature for 3 h, and then excess particles were washed with deionized water. The 3-point bend test was carried out using a universal testing machine; the tested specimen has 50 mm of span length and 1 mm of thickness. The UTM has a maximum load cell capacity of 5 kN, and 0.00001 s^{-1} of strain rate was used throughout the test. A Digital Storage Oscilloscope (Tektronix 1072B) was used to record the voltage output upon the application of various external forces on the device.

2.2. Theoretical Methods. DFT calculations for these systems were done with the Vienna ab initio simulation (VASP) package.[22] The electron−ion interactions were described using all-electron projector-augmented wave pseudopotentials,[23] and Perdew−Burke−Ernzerhof (PBE) generalized gradient approximation (GGA)[24] was used to approximate the electronic exchange and correlations. The plane-wave kinetic energy cutoffs of 580 and 520 eV were used for bulk ZnO and all other calculations, respectively. The Brillouin zone was sampled using 8 × 8 × 8, 8 × 1 × 1, 8 × 8 × 1, and 5 × 5 × 1 Monkhorst−Pack *k*-grids for bulk ZnO, polylactic acid, density of states, and all other calculations, respectively. All of the structures were relaxed using a conjugate gradient scheme until the energies and each component of the forces converged to 10^{-7} eV and 0.001 eV Å^{-1} for bulk ZnO and 10^{-5} eV and 0.01 eV Å^{-1} for all other calculations, respectively. All of the calculations are spin-polarized and dipole-corrected.

3. RESULTS AND DISCUSSION

The overall fabrication process of the ZnO nanosheets on a 3D-printed polymeric fabric is presented schematically in Figure 1a.

https://doi.org/10.1021/acsami.3c08374
ACS Appl. Mater. Interfaces 2023, 15, 44513−44520

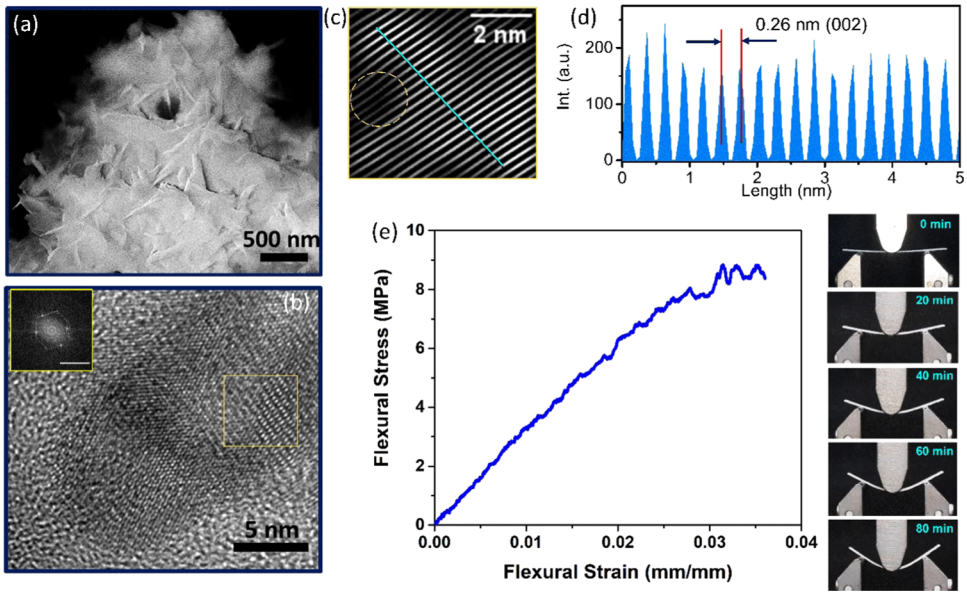

Figure 2. (a) FESEM image of the ZnO-coated 3D-printed hex structure. (b) TEM image of ZnO nanosheets. The inset shows the electron diffraction pattern. (c) HRTEM image of ZnO nanosheets. Circle denotes the presence of defects in the material. (d) Lattice spacing of ZnO nanosheets. (e) Flexural stress−strain of the 3D-printed hex structure. Snapshots of the 3D-printed hex structure under bending stress.

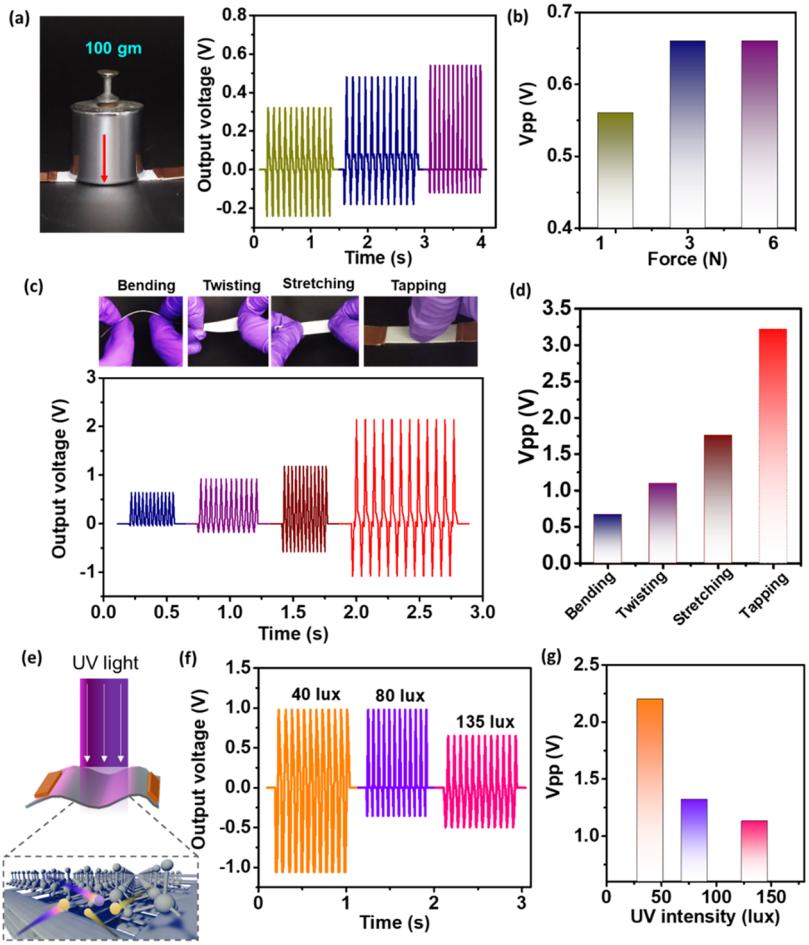

Figure 3. (a) Digital photograph of loading on the 3DP device. Force-dependent piezoresponse. (b) Peak-to-peak voltage of the ZnO-decorated 3DP hex structure under various applied forces. (c) Piezoelectricity under different types of mechanical stimulus. The upper inset shows the digital photographs of the device during different experimental conditions. (d) Peak-to-peak voltage of the 3DP piezoelectric system under various types of forces. (e) Schematic presentation of the UV light intensity-dependent piezoelectricity and (f) output response under UV light illumination. (g) Peak-to-peak voltage under various UV light intensities.

https://doi.org/10.1021/acsami.3c08374
ACS Appl. Mater. Interfaces 2023, 15, 44513−44520

The detailed synthesis method was described in our previous report.[25] First, the 3D-printed hex substrate was printed (see Section 2 for more details) with dimensions of 50 mm × 50 mm × 1 mm (Figure 1b). After that, the 3D-printed substrate was immersed into the zinc salt and NaOH solution under 90 °C for 2 h and the solution pH was maintained at ∼10. The uniform ZnO nanosheet-decorated 3D-printed scaffold was then obtained. The optical microscopy measurement was carried out to study the surface porosity at a microscopic level, and we found the overlaying of 3D-printed layers with oval pores on the surface (Figure S2). Apart from that, we have observed the surface roughness, which can provide an excellent site for the in situ growth of ZnO nanosheets. Figure S3 shows the optical microscopy image of a ZnO-coated 3D-printed fabric. Further, the FESEM morphology has been studied to observe the surface interaction between ZnO nanosheets and PLA (Figure S4a). It clearly shows the growth of ZnO nanosheets on the polymer fabric. In order to further probe the distribution of the elements after coating, we studied elemental composition using energy-dispersive X-ray (EDX) spectra as shown in Figure S4b. It shows the presence of C, O, and Zn. The elemental color mapping further confirms the distribution of all of the elements in the interface. The FESEM image of nanosheets is shown in Figure 2a, and the results confirm the in situ growth of thin ZnO on the polymer surface with a lateral dimension of ∼500−700 nm.[25] To further confirm the formation of thin sheets, TEM analysis was done, and it conforms to the crystallinity of ZnO layers (Figure 2b). Such thin nanostructures with a large specific surface area should significantly enhance the effective contact area, which increases the charge transfer inside the interface. The electron diffraction pattern, as shown in the inset of Figure 2b, confirms the hexagonal crystal structure of the synthesized 2D ZnO. Additionally, the high-resolution TEM (HRTEM) image confirms the presence of surface defects in the nanosheets (denoted by a dotted yellow square box) (Figure 2c). Figure 2d shows the interplanar spacing of ∼0.26 nm corresponding to the (002) plane of hexagonal ZnO. In order to determine the chemical composition of the material, we also performed an X-ray photoelectron spectroscopy (XPS) measurement (Figure S5). The full-scan XPS profile of the 2D ZnO clearly confirms the presence of zinc and oxygen in the sample. To understand the flexibility of the 3D-printed hex structure, we carried out the 3-point bend test (flexural test) (Figure 2e). The flexural stress−strain curve shows that the as-tested 3D-printed hex structure has a flexural modulus and flexural stress of 334.8 and 8.8 MPa, respectively. The maximum flexural load is recorded at 0.03146 of flexural strain. To study the deformation behavior, we have captured snapshots of the test at a specific interval (20 min) and found the uniform deformation of the structure (right panel of Figure 2e).

To evaluate the combined responses of piezoelectric and triboelectric effects in the 3D-printed architecture, the generated output response was measured at different external forces with a repetition rate of ∼5 Hz. The output response was recorded for three different applied forces of ∼1, 3, and 6 N (right side of Figure 3a and Video S1) under uniform cyclic loading. The peak-to-peak voltage (V_{pp}) was calculated, and the response is directly proportional to the applied mechanical force (Figure 3b) with a maximum voltage of ∼0.65 V. In this instance, we have seen that the output voltages are nearly saturated after ∼5 N of applied force, which may indicate that the force is sufficient to maximize the transfer of charges on the surface of the polymer and material contact. The digital snapshot (Figure 3a) shows the loading condition on the 3DP system. The output voltages were also measured in relation to changing load resistances (R_L), and the results are depicted in Figure S3. As a result, the estimated output power density $\left(P \sim \frac{V^2}{R_L}\right)$ across ∼10 MΩ (R_L) was ∼52 nW/cm^2 with an electrode size of 5 cm^2. So, such output power and sensing capabilities may be used to power semiconductor technology, such as medical applications for remote health monitoring.

The fabricated flexible 3DP system can be further used as a smart system and is capable of generating output voltage under different mechanical conditions. To demonstrate this, different external loading conditions, such as bending, twisting, stretching, and tapping, were employed. The resulting output voltage was collected at each of the condition as shown in Figure 3c. We have observed that tapping has exerted the highest V_{pp} among all of them. The V_{pp} voltage exerted by finger tapping is almost ∼6 times higher than the bending condition. The V_{pp} voltage is found to increase in the following order bending < twisting < stretching < tapping (Figure 3d). The ZnO/polymer interface experienced a significant strain under these conditions, as most of the stain is concentrated in the interface rather than the individual ZnO and polymer matrix. Here, two different materials are physically in contact at the interface and mechanically impact one another, which can cause a charge exchange that produces an electrostatic potential. Positive and negative charges are produced on ZnO nanosheets and polymer matrix when the 3DP fabric is continuously bent, twisted, stretched, and tapped.[26−28] Under these conditions, ZnO has physical contact with the polymer fabric and leads to charge separation and transportation. The piezoelectric nature in ZnO nanosheets was observed mainly due to the presence of oxygen defect and defect migration.[29−31] Because of the high sensitivity and fast response ($\tau \sim 2$ ms), the ultrathin ZnO-based nanogenerator is therefore designed specifically for sensing a very small amount of force. The displacement/rotation of Zn^{2+} with respect to that of O^{2-} causes the generation of a piezopotential inside the materials in response to an externally applied compressive force. Table S1 summarizes the findings and the existing viewpoints on the output performance of ZnO-based nanogenerators and their piezoelectric effects for comparison. We found that under mechanical stress, the atomically thin ZnO and polymer interface generates more effective output. Further, to confirm the presence of surface oxygen and surface defects in the nanosheets, the output response of the 3DP fabric was measured under UV light (λ = 365 nm) illumination. The presence of surface states and native defects has found a strongly modulated carrier density, which affects the output response at the interface. The voltage response under different UV light intensities, such as 40, 80, and 120 lx, was measured to determine the impact of UV light on ZnO nanosheets (Figure 3e,f). The response of the piezoelectric output voltage from the printed architecture is inversely proportional to the UV light intensity as shown in Figure 3g. Under white light illumination, ZnO shows low conductivity at the surface, as oxygen molecules are absorbed on the surface, which facilitates capturing free electrons from the conduction band of ZnO. However, under UV light illumination, electron−hole pairs are generated in the material and hole migrates to the surface and neutralized the oxygen ions and the remaining free electron generates in the conduction channels. In the case of higher UV light intensity, the concentration of electron−hole in the ZnO increases, but due to limited oxygen on the surface, all

https://doi.org/10.1021/acsami.3c08374
ACS Appl. Mater. Interfaces 2023, 15, 44513−44520

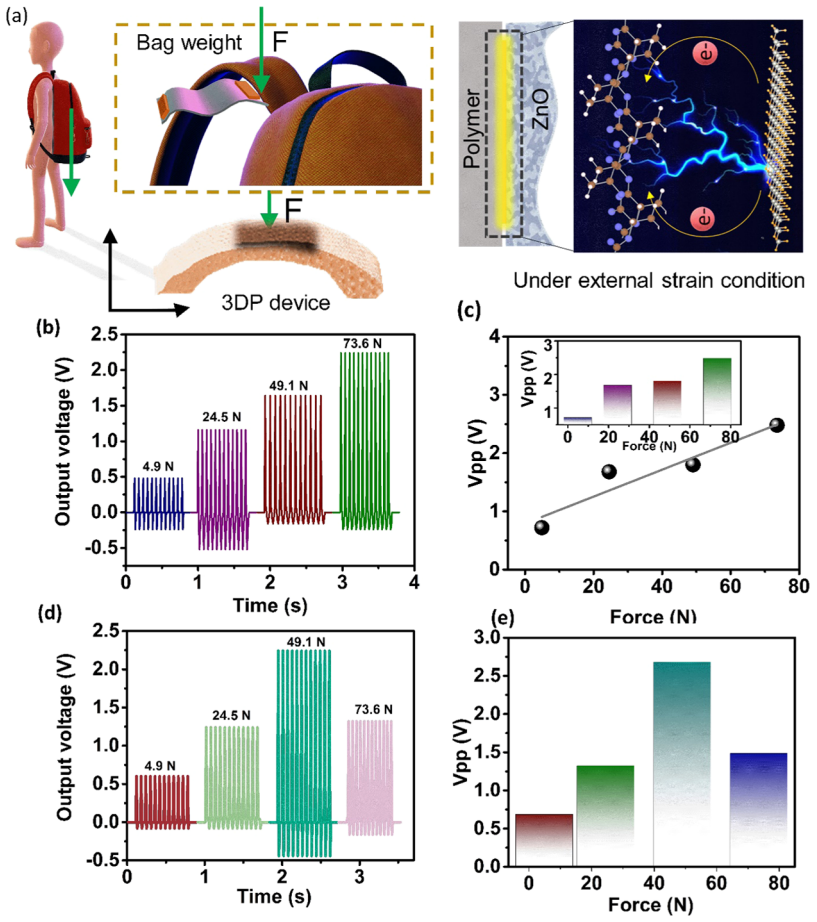

Figure 4. (a) Schematic illustration of external impacts on the bag shoulder and charge-transfer mechanism under external strained conditions. (b) High static force-dependent output response. (c) Linear relationship between the peak-to-peak voltage of 3DP hex structure and various high static forces. The inset shows the bar plot of output voltage under different loadings. (d) High dynamic force-dependent voltage output. (e) Peak-to-peak voltage of the 3DP system under various high dynamic forces.

of the holes cannot be stabilized. Therefore, at some points, free electron density does not increase and it even suppresses the generation of free electrons/carries.[32]

Previously, several efforts were devoted to the fabrication of energy harvesting devices using different flexible substrates such as cotton, polymers, papers, etc. However, preparing of highly sensitive devices with stability is still a challenge.[33] Taking advantage of the distinct architecture with high flexibility, as a proof-of-concept, the 3DP architecture was used to measure the responses by utilizing it in the padded shoulder strap of the school bag under both the conditions, standing (static) and walking (dynamic) (Figure 4a). The empty bag provides ~5 N force, and then additional force was applied along with the backpack, which makes the total force to ~25, 50, and 75 N. The hybrid response of the 3D-printed structure under high static force is shown in Figure 4b. The peak-to-peak voltage is directly proportional to the applied force (Figure 4c). A linear increment of the output voltage was observed here. We also calculated the mechanical sensitivity of the 3DP architecture, and it is found to be ~0.023 V/N for the maximum weight of the bag. The charge generation occurs at the ZnO surface under strain condition, and electron transfer occurs when the polymer contacts with the ZnO surface (right side of Figure 4a). When the external force is applied to a piezoelectric material (ZnO nanosheet), the piezoelectric charges appear on the surface. At this time, the triboelectrification mechanism also starts to function. When the potential difference between the materials is balanced (in equilibrium), the polarized charges are transferred from ZnO to the polymer matrix. Due to the nature of the simultaneous triboelectric and piezoelectric effects, the signal should increase, and the result proves that the signal totally comes from both the effects. Similarly, the output response of the 3D-printed structure under high dynamic force (walking with a bag) is shown in Figure 4d and Video S2. However, V_{pp} is increased from 5 to 50 N force and then decreased at 75 N force (Figure 4e). We also studied the stability of the 3DP fabric under different experimental conditions (Figure S7). During the stability measurement, the fabric shows a similar amplitude of V_{pp}, which confirms that the fabricated device can be used for practical applications. Further, to compare the output voltage bare PLA and ZnO-coated 3DP devices, we have measured the V_{pp} as shown in Figure S8 and Video S1. This confirms the poor performance of bare PLA compared to that of the 3DP device.

To shed light on the interaction of ZnO nanosheets and the polymer interface as a better energy harvester compared to bare PLA, density functional theory (DFT) calculations were performed. Corresponding results about the constructive contribution of triboelectric and piezoelectric effects in the interface and the charge distribution in ZnO nanosheets under various pressures are shown in Figure 5. A monolayer of ZnO was created starting from the bulk structure of ZnO with optimized lattice parameters $a = b = 3.28$ Å and $c = 5.30$ Å. This

https://doi.org/10.1021/acsami.3c08374
ACS Appl. Mater. Interfaces 2023, 15, 44513−44520

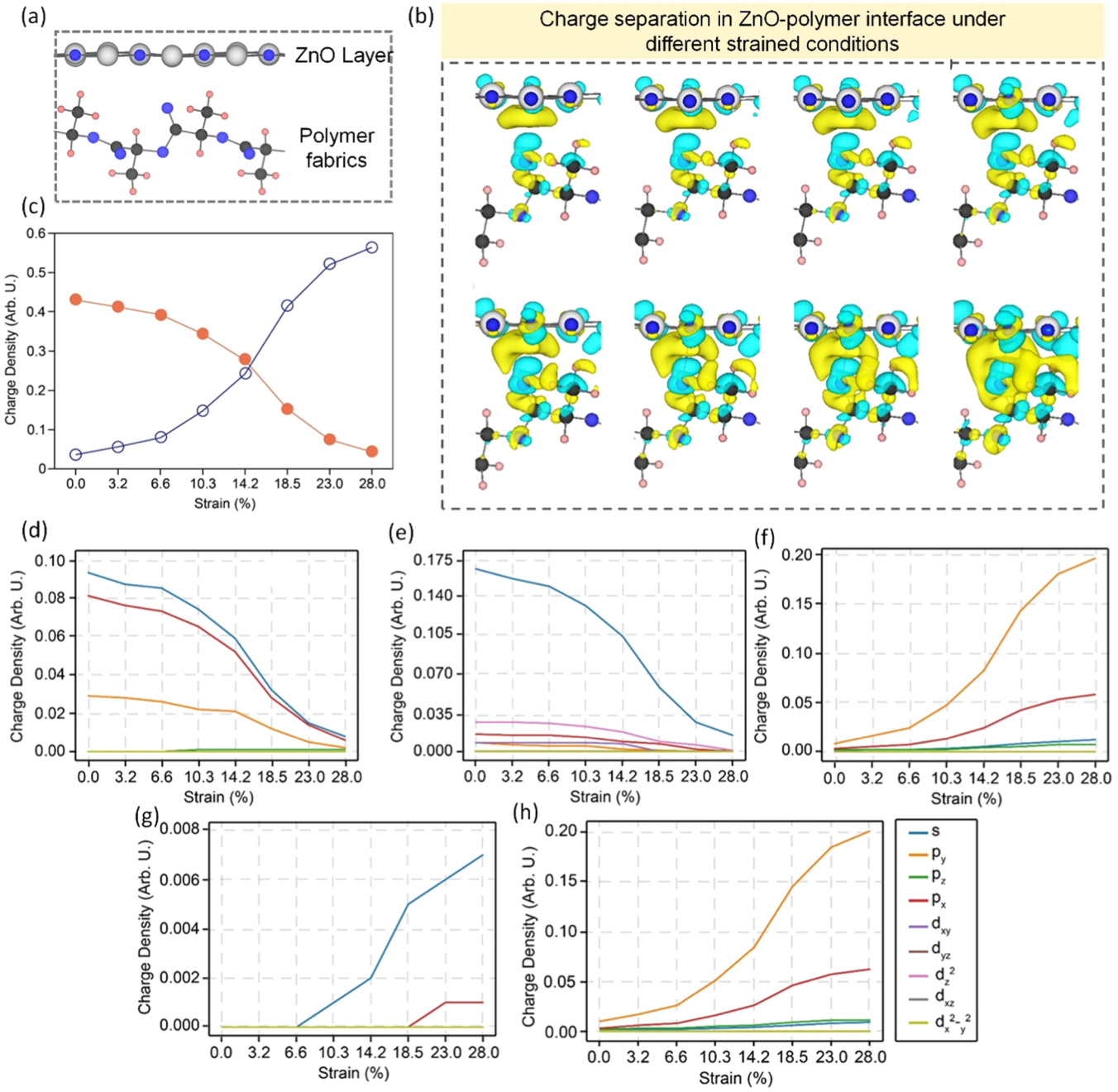

Figure 5. (a) Theoretical structure of the ZnO−polymer interface. Charge separation diagram of the ZnO/PLA heterostructure under (b) unstrained condition (upper panel left) 3.2, 6.6, 10.3, 14.2, 18.5, 23.0, and 28.0% normal strain where the yellow and blue regions indicate the electron-depleted and -accepted regions, respectively. (c) Charge density at the conduction band as a function of normal strain: charge density at the conduction band as a function strain for (d) O (ZnO), (e) Zn (ZnO), (f) O (PLA), (g) H (PLA), and (h) C (PLA).

monolayer of ZnO was placed over the optimized PLA structure where the distance between the top of PLA and ZnO is 1.92 Å after optimization (Figure 5a). The Theoretical Methods section contains a description of the simulation's specifics. The following normal strain (3.2, 6.6, 10.3, 14.2, 18.5, 23.0, and 28.0%) was then applied to the ZnO/polymer heterostructure at an interval of 0.06 Å up to 1.50 Å. The corresponding strained structures were allowed to be optimized in only the *x,y*-plane. The charge analysis diagram for unstrained and all strained structures shows that with increasing strain the charge separation between ZnO and fabric increases where the ZnO donates electrons to the polymer (Figure 5b). Therefore, it confirms the increasing interlayer interaction between ZnO and fabric with increasing normal strain. When the polymer comes in contact with ZnO nanosheets with increasing pressure, charge transfer takes place at the interface.[33,34] Further, to understand the change in the contribution of ZnO and polymer to the conduction band (CB) with increasing strain, we plotted the charge density diagram of the conduction band minimum (CBM) at a particular *K*-point (Figure 5c,h). The contribution of PLA electronic states in CBM is less than that of the ZnO. On further increasing strain up to 28.0%, the contribution of ZnO electronic states in CBM decreases rapidly, whereas it proportionally increases for PLA. At an 18.5% strain, the

https://doi.org/10.1021/acsami.3c08374
ACS Appl. Mater. Interfaces 2023, 15, 44513−44520

contribution of ZnO electronic states in CBM becomes higher than that of the PLA. In the unstrained heterostructure, s and p_y orbitals of the O and s orbitals of the Zn of ZnO have the maximum contribution in CBM. However, their contribution decreases with increasing strain, whereas the participation from the p_y orbital of the O and C atoms of PLA enhances with negligible share from the H atom. Analyzing the PLA structure with respect to the C−O and C═O bond lengths of the (−C(−O−)═O) group as depicted in Figure S9a, the C−O bond length is around 1.36 Å. This bond length is in between the C═O (1.23 Å) and C−O (1.45 Å). This confirms the resonating electrons between the ether oxygen and carbonyl oxygen, which is expected to decrease the urge to accept electrons from ZnO by the carbonyl oxygen. However, the existing resonating electron delocalization direction is reversed in the heterostructure, where the electron is accepted (Figure S9b). This is further confirmed by the increasing charge density on the p_y orbital of both C and O on the PLA structure with respect to the enhanced strain (Figure 5f,h). The 3DP ZnO fabric heterostructure exhibits synergistic capabilities for energy production as a result. The charge distribution under the application of strain is determined by the structural design. Experimentally, we observed that the maximum output voltage varied according to the stress distribution. According to our findings, altering the polymer substrate design can be used to adjust the maximum strain as well as the energy harvesting capability. However, if the maximum stress reaches the yield strength of the material, the sensor exhibits high hysteresis; subsequently, the durability decreases.

4. CONCLUSIONS

In conclusion, we have studied how the polymer−semiconductor heterojunctions may impact the piezoelectric−triboelectric responses using 2D ZnO as models. We demonstrated unequivocally that the improved output response is caused by a significant electrostatic interaction between 2D ZnO and the PLA polymer. The 2D nature of ZnO easily transports this locally produced net polarization into the polymer, exhibiting outstanding energy harvesting abilities. According to the DFT calculations, the 2D ZnO and PLA had strong electrostatic interactions, which may lead to the development of efficient energy harvesting devices. Our detailed insight into the nanoscale charge separation mechanism at the interface between a polymer and a 2D sheet may help to develop the composites with a wider range of applications, including wearable energy harvesting.

■ ASSOCIATED CONTENT

Supporting Information

The Supporting Information is available free of charge at https://pubs.acs.org/doi/10.1021/acsami.3c08374.

Optical microscopy images of the device (Figures S1−S3); interface analysis of ZnO and polymer by using FESEM and EDX data (Figure S4); XPS data (Figure S5); output voltage vs load resistance and stability (Figures S6 and S7); comparison of the output voltage (Figure S8); and comparison of the current research with various ZnO nanostructures (Table S1) (PDF)

Piezoelectric response of bare PLA and ZnO-coated PLA hex structures (MP4)

Piezoelectric response of the ZnO-coated PLA hex structure in static and dynamic conditions (MP4)

■ AUTHOR INFORMATION

Corresponding Authors

Debmalya Roy − *Directorate of Nanomaterials, DMSRDE, Kanpur 208013 Uttar Pradesh, India;* orcid.org/0000-0003-3629-5309; Email: droy.dmsrde@gov.in

Abhishek K. Singh − *Department of Materials Engineering, Indian Institute of Science, Bangalore 560012 Karnataka, India;* orcid.org/0000-0002-7631-6744; Email: abhishek@iisc.ac.in

Chandra S. Tiwary − *Department of Metallurgical and Materials Engineering, Indian Institute of Technology Kharagpur, Kharagpur 721302 West Bengal, India;* orcid.org/0000-0001-9760-9768; Email: chandra.tiwary@metal.iitkgp.ac.in

Authors

Partha Kumbhakar − *Department of Metallurgical and Materials Engineering, Indian Institute of Technology Kharagpur, Kharagpur 721302 West Bengal, India; Department of Physics and Electronics, CHRIST (Deemed to be University), Bangalore 560029, India;* orcid.org/0000-0003-1001-9349

Rushikesh S. Ambekar − *Department of Metallurgical and Materials Engineering, Indian Institute of Technology Kharagpur, Kharagpur 721302 West Bengal, India*

Arko Parui − *Department of Materials Engineering, Indian Institute of Science, Bangalore 560012 Karnataka, India*

Ajit K. Roy − *Materials and Manufacturing Directorate, Air Force Research Laboratory, Wright Patterson AFB, Ohio 45433-7718, United States*

Complete contact information is available at: https://pubs.acs.org/10.1021/acsami.3c08374

Author Contributions

#P.K., R.S.A., and A.P. contributed equally to this work. All of the authors participated in the analysis and manuscript writing.

Notes

The authors declare no competing financial interest.

■ ACKNOWLEDGMENTS

C.S.T. acknowledges Core research grant of SERB, India, STARS project by MHRD-India, DAE Young Scientist Research Award (DAEYSRA), and AOARD (Asian Office of Aerospace Research and Development) grant nos. FA2386-21-1-4014 and FA2386-23-1-4034.

■ ABBREVIATIONS

2D, two-dimensional; 3D, three-dimensional; vdW, van der Waals; SEM, scanning electron microscope; XRD, X-ray diffraction; UV, ultraviolet; DFT, density functional theory; PLA, polylactic acid; UTM, universal testing machine; PBE, Perdew−Burke−Ernzerhof; GGA, generalized gradient approximation; TEM, transmission electron microscopy; V_{pp}, peak-to-peak voltage; 3DP, three-dimensional printing; CBM, conduction band minimum

■ REFERENCES

(1) World Population Prospects https://population.un.org/wpp/Publications/Files/WPP2019_Highlights.pdf (accessed Jan 11, 2022).
(2) Data and Statistics https://www.iea.org/data-and-statistics (accessed Jan 11, 2022).
(3) Global Energy Review 2021: CO_2 emissions https://www.iea.org/reports/global-energy-review-2021/co2-emissions#abstract.

(4) Barnham, K. W. J.; Mazzer, M.; Clive, B. Resolving the Energy Crisis: Nuclear or Photovoltaics? *Nat. Mater.* **2006**, *5* (3), 161−164.
(5) Lee, M.; Chen, C. Y.; Wang, S.; Cha, S. N.; Park, Y. J.; Kim, J. M.; Chou, L. J.; Wang, Z. L. A Hybrid Piezoelectric Structure for Wearable Nanogenerators. *Adv. Mater.* **2012**, *24* (13), 1759−1764.
(6) Yao, D.; Cui, H.; Hensleigh, R.; Smith, P.; Alford, S.; Bernero, D.; Bush, S.; Mann, K.; Wu, H. F.; Chin-Nieh, M.; Youmans, G.; Zheng, X. Achieving the Upper Bound of Piezoelectric Response in Tunable, Wearable 3D Printed Nanocomposites. *Adv. Funct. Mater.* **2019**, *29* (42), No. 1903866.
(7) Ambekar, R. S.; Kushwaha, B.; Sharma, P.; Bosia, F.; Fraldi, M.; Pugno, N. M.; Tiwary, C. S. Topologically Engineered 3D Printed Architectures with Superior Mechanical Strength. *Mater. Today* **2021**, *48*, 72−94.
(8) Hu, L.; Pasta, M.; La Mantia, F.; Cui, L.; Jeong, S.; Deshazer, H. D.; Choi, J. W.; Han, S. M.; Cui, Y. Stretchable, Porous, and Conductive Energy Textiles. *Nano Lett.* **2010**, *10* (2), 708−714.
(9) Jost, K.; Stenger, D.; Perez, C. R.; McDonough, J. K.; Lian, K.; Gogotsi, Y.; Dion, G. Knitted and Screen Printed Carbon-Fiber Supercapacitors for Applications in Wearable Electronics. *Energy Environ. Sci.* **2013**, *6* (9), 2698.
(10) Liang, J.; Zeng, H.; Qiao, L.; Jiang, H.; Ye, Q.; Wang, Z.; Liu, B.; Fan, Z. 3D Printed Piezoelectric Wound Dressing with Dual Piezoelectric Response Models for Scar-Prevention Wound Healing. *ACS Appl. Mater. Interfaces* **2022**, *14* (27), 30507−30522.
(11) Huang, Q.; Wang, D.; Zheng, Z. Textile-Based Electrochemical Energy Storage Devices. *Adv. Energy Mater.* **2016**, *6* (22), No. 1600783.
(12) Carlos, C.; Li, J.; Zhang, Z.; Berg, K. J.; Wang, Y.; Wang, X. Strain-Correlated Piezoelectricity in Quasi-Two-Dimensional Zinc Oxide Nanosheets. *Nano Lett.* **2023**, *23* (13), 6148−6155.
(13) Yan, M.; Li, H.; Liu, S.; Xiao, Z.; Yuan, X.; Zhai, D.; Zhou, K.; Bowen, C. R.; Zhang, Y.; Zhang, D. 3D-Printed Flexible PVDF-TrFE Composites with Aligned BCZT Nanowires and Interdigital Electrodes for Piezoelectric Nanogenerator Applications. *ACS Appl. Polym. Mater.* **2023**, *5* (7), 4879−4888.
(14) Thi, Q. H.; Kim, H.; Zhao, J.; Ly, T. H. Coating Two-Dimensional MoS2 with Polymer Creates a Corrosive Non-Uniform Interface. *npj 2D Mater. Appl.* **2018**, *2* (1), No. 34.
(15) Zhang, G.; Liao, Q.; Ma, M.; Gao, F.; Zhang, Z.; Kang, Z.; Zhang, Y. Uniformly Assembled Vanadium Doped ZnO Microflowers/Bacterial Cellulose Hybrid Paper for Flexible Piezoelectric Nanogenerators and Self-Powered Sensors. *Nano Energy* **2018**, *52*, 501−509.
(16) Lee, Y.; Kim, S.; Kim, D.; Lee, C.; Park, H.; Lee, J.-H. Direct-Current Flexible Piezoelectric Nanogenerators Based on Two-Dimensional ZnO Nanosheet. *Appl. Surf. Sci.* **2020**, *509*, No. 145328.
(17) Manjula, Y.; Rakesh Kumar, R.; Swarup Raju, P. M.; Anil Kumar, G.; Venkatappa Rao, T.; Akshaykranth, A.; Supraja, P. Piezoelectric Flexible Nanogenerator Based on ZnO Nanosheet Networks for Mechanical Energy Harvesting. *Chem. Phys.* **2020**, *533*, No. 110699.
(18) Supraja, P.; R, R. K.; Mishra, S.; Haranath, D.; Sankar, P. R.; Prakash, K. A Simple and Low-Cost Approach for the Synthesis and Fabrication of ZnO Nanosheet-Based Nanogenerator for Energy Harvesting and Sensing. *Eng. Res. Express* **2021**, *3* (3), No. 035022.
(19) Gong, S.; Schwalb, W.; Wang, Y.; Chen, Y.; Tang, Y.; Si, J.; Shirinzadeh, B.; Cheng, W. A Wearable and Highly Sensitive Pressure Sensor with Ultrathin Gold Nanowires. *Nat. Commun.* **2014**, *5* (1), No. 3132.
(20) Chen, C.; Wang, X.; Wang, Y.; Yang, D.; Yao, F.; Zhang, W.; Wang, B.; Sewvandi, G. A.; Yang, D.; Hu, D. Additive Manufacturing of Piezoelectric Materials. *Adv. Funct. Mater.* **2020**, *30* (52), No. 2005141.
(21) Alexander, R. M.; Bennet-Clark, H. C. Storage of Elastic Strain Energy in Muscle and Other Tissues. *Nature* **1977**, *265* (5590), 114−117.
(22) Kresse, G.; Hafner, J. Ab Initio Molecular Dynamics for Liquid Metals. *Phys. Rev. B* **1993**, *47* (1), 558−561.
(23) Kresse, G.; Joubert, D. From Ultrasoft Pseudopotentials to the Projector Augmented-Wave Method. *Phys. Rev. B* **1999**, *59* (3), 1758−1775.
(24) Perdew, J. P.; Burke, K.; Ernzerhof, M. Generalized Gradient Approximation Made Simple. *Phys. Rev. Lett.* **1996**, *77* (18), 3865−3868.
(25) Kumbhakar, P.; Ambekar, R. S.; Mahapatra, P. L.; Sekhar Tiwary, C. Quantifying Instant Water Cleaning Efficiency Using Zinc Oxide Decorated Complex 3D Printed Porous Architectures. *J. Hazard. Mater.* **2021**, *418*, No. 126383.
(26) Soin, N.; Zhao, P.; Prashanthi, K.; Chen, J.; Ding, P.; Zhou, E.; Shah, T.; Ray, S. C.; Tsonos, C.; Thundat, T.; Siores, E.; Luo, J. High Performance Triboelectric Nanogenerators Based on Phase-Inversion Piezoelectric Membranes of Poly(Vinylidene Fluoride)-Zinc Stannate (PVDF-ZnSnO3) and Polyamide-6 (PA6). *Nano Energy* **2016**, *30*, 470−480.
(27) Liu, S.; Zheng, W.; Yang, B.; Tao, X. Triboelectric Charge Density of Porous and Deformable Fabrics Made from Polymer Fibers. *Nano Energy* **2018**, *53*, 383−390.
(28) Zbigniew Bończa-Tomaszewski, P. P. Tribo Charging Powder Coatings. *Macromol. Symp.* **2002**, *187* (1), 417−426.
(29) Jacobi, K.; Zwicker, G.; Gutmann, A. Work Function, Electron Affinity and Band Bending of Zinc Oxide Surfaces. *Surf. Sci.* **1984**, *141* (1), 109−125.
(30) Feng, Y.; Li, W.-L.; Xu, D.; Qiao, Y.-L.; Yu, Y.; Zhao, Y.; Fei, W.-D. Defect Engineering of Lead-Free Piezoelectrics with High Piezoelectric Properties and Temperature-Stability. *ACS Appl. Mater. Interfaces* **2016**, *8* (14), 9231−9241.
(31) Kumbhakar, P.; Mukherjee, M.; Pramanik, A.; Karmakar, S.; Singh, A. K.; Tiwary, C. S.; Kumbhakar, P. Confinement Aided Simultanous Water Cleaning and Energy Harvesting Using Atomically Thin Wurtzite (Wurtzene). *Adv. Sustainable Syst.* **2021**, *5* (2), No. 2000189.
(32) Pham, T. T.; Lee, K. Y.; Lee, J.-H.; Kim, K.-H.; Shin, K.-S.; Gupta, M. K.; Kumar, B.; Kim, S.-W. Reliable Operation of a Nanogenerator under Ultraviolet Light via Engineering Piezoelectric Potential. *Energy Environ. Sci.* **2013**, *6* (3), 841.
(33) Mahapatra, P. L.; Singh, A. K.; Lahiri, B.; Kundu, T. K.; Roy, A. K.; Kumbhakar, P.; Tiwary, C. S. Energy Harvesting Using Cotton Fabric Embedded with 2D Hexagonal Boron Nitride. *ACS Appl. Mater. Interfaces* **2022**, *14* (26), 30343−30351.
(34) Yousry, Y. M.; Yao, K.; Mohamed, A. M.; Liew, W. H.; Chen, S.; Ramakrishna, S. Theoretical Model and Outstanding Performance from Constructive Piezoelectric and Triboelectric Mechanism in Electrospun PVDF Fiber Film. *Adv. Funct. Mater.* **2020**, *30* (25), No. 1910592.

https://doi.org/10.1021/acsami.3c08374
ACS Appl. Mater. Interfaces 2023, 15, 44513−44520